Robotica: (2020) volume 38, pp. 1642–1664. © Cambridge University Press 2019
doi:10.1017/S026357471900167X

Adaptive Sliding Mode Impedance Control of Single-Link Flexible Manipulators interacting with the Environment at an Unknown Intermediate Point

Ali Fayazi†*, Naser Pariz‡¶, Ali Karimpour‡¶, V. Feliu-Batlle‡¶ and S. Hassan HosseinNia‡¶§

†*Department of Electrical Engineering, Vali-e-Asr University of Rafsanjan, Rafsanjan, Iran*
‡*Department of Electrical Engineering, Ferdowsi University of Mashhad, Mashhad, Iran*
¶*Department of Electrical, Electronics, and Control Engineering, University of Castilla-La Mancha, Ciudad Real 13071, Spain*
§*Department of Precision and Microsystems Engineering, Delft University of Technology, Delft, Netherlands*

(Accepted October 19, 2019. First published online: November 25, 2019)

SUMMARY
This paper proposes an adaptive robust impedance control for a single-link flexible arm when it encounters an environment at an unknown intermediate point. First, the intermediate collision point is estimated using a collision detection algorithm. The controller, then, switches from free to constrained motion mode. In the unconstrained motion mode, the exerted force to environment is nearly zero. Thus, the reference trajectory is a prescribed desired trajectory in position control. In the constrained motion mode, the reference trajectory is determined by the desired target dynamic impedance. The simulation results demonstrate the efficiency of proposed control scheme.

KEYWORDS: Impedance control; Adaptive sliding mode controller; Single-link flexible manipulators; Unknown intermediate point; Disturbance observer.

1. Introduction

Flexible robots are widely used in various applications, such as aerospace, medicine, industry, etc. Flexible robots are mainly introduced with at least one flexible element in their mechanical structure. Flexible robots have several advantages over the conventional rigid robots which include the higher speed operation, lower energy consumption, faster maneuverability, better transportability, and higher payload-to-arm weight ratio. In spite of these useful characteristics, due to the extensive structural flexibility, the modeling and control of the flexible robots are more complicated over rigid ones.

Recently, flexible links have been utilized extensively in various new robotic applications. Important among these applications are the following: industrial new robotics applications with a focus on the use of lightweight materials; aerospace industry application in which the lightweight of the manipulators is an essential requirement;[1] motion control of large structures, such as boom cranes and fire rescue turntable ladders, which are treated as flexible link robots;[2] motion control of

* Corresponding author. E-mail: a.fayazi@vru.ac.ir

a sensing antenna that slides on a surface and detects an object.[3,4] Modeling, control, and some of the most important applications of the flexible manipulators have been reviewed in refs. [5–9]. Three control algorithms which are mainly used to accomplish tasks that involve constrained motions are impedance control, admittance control, and hybrid position/force control. The idea of impedance control first proposed by Hogan.[10]

In the recent decades, various control approaches into flexible manipulator interacting with the environment have been proposed.[11–19] Some of these control strategies are in relation to the force control of the flexible robot. Moreover, in the last two decades, impedance control of the rigid manipulators interacting with the environment has been widely reviewed that can be found in the scientific literature.[20–29] However, the robust impedance control of the flexible manipulator has been rarely addressed by the researcher.[30–34] In ref. [15], force control of a lightweight single-link flexible arm is presented based on coupling torque feedback. In ref. [30], the modeling and impedance control of a single-link flexible arm are proposed for both constrained and unconstrained movements through sliding mode control algorithm. In ref. [34], robust impedance control of a single-link flexible manipulator interacting with the unknown environment is proposed using sliding mode control which is valid for both unconstrained and constrained maneuvers.

In many articles which are related to the control of a single-link flexible arm interacting with the environment, for example, in refs. [15,30], two separate controller are suggested to control the system for two different operating modes (free and constrained motion). Therefore, two different dynamic models should also be available for this operating modes. A collision detection algorithm is also required for switching the controller from the unconstrained to the constrained motion mode. In addition, the environment parameters (stiffness and damping coefficient) have to be known. Moreover, in most of the research done with the subject of the impedance control of the flexible manipulators, the contact point is usually considered at the end point of the manipulator. Whereas, there is a lack of study on impedance control of the flexible manipulators with collision at an unknown intermediate point. The ultimate aim of this paper is to apply an adaptive robust impedance control method to the single-link flexible manipulators interacting with the environment with collision at an unknown intermediate point of the manipulator. In our novel approach, the controller automatically switches from the free to the constrained motion mode; therefore, it does not need an algorithm to detect collision between the link and environment. In this regard, an impedance control is proposed based on the position control. This means that in the free motion, the applied force to the environment is zero and the reference trajectory for the position control block is the desired trajectory. Whereas, in the constrained motion mode, the reference trajectory for the position control block is determined by the desired impedance dynamics.

This paper is structured as follows. Section 2 describes the modeling of the single-link flexible arm. Section 3 introduces the adaptive robust impedance control algorithm which is based on the sliding mode control method. Sections 4 and 5 present the stability analysis of closed-loop control system and the definitions of the performance criteria. Section 6 provides the simulation results to depict the effectiveness of our proposed control scheme. Finally, Section 7 presents our conclusions.

2. Dynamic Modeling of a Single-Link Flexible Manipulator System

In general, there are two methods which can be used to drive the single-link flexible manipulator dynamics. The first method is based on ordinary differential equations, which are derived using approximation methods such as the lumped parameter model,[35] the lumped mass model,[36] or the truncation of a distributed parameter model.[37] The second method is based on partial differential equation dynamic models which can accurately reflect the dynamic features of flexible manipulators.[38,39] In the following, the single-link flexible manipulator dynamics and DC motor dynamics are described.

2.1. Link dynamics: Constrained motion with collision at the intermediate points

In this section, the lumped mass model is used to obtain the reduced flexible link dynamics with tip mass in order to achieve a simple and convenient design control.[15] The dynamics model of a single-link flexible arm with collision at the end point is presented in ref. [34]. In this work, we pursue to derive the dynamics model for a single-link flexible manipulator with collision at an intermediate point. Figure 1 depicts the parametric representation of a single-link flexible arm in constrained motion mode when it comes into contact with the environment at an intermediate point.

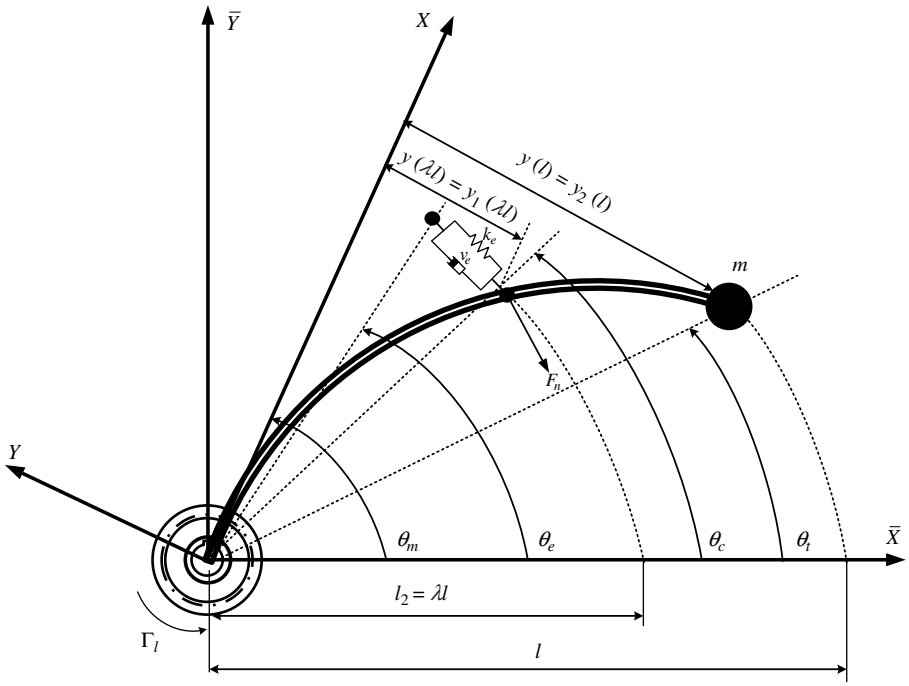

Fig. 1. Single-link flexible arm with collision at an unknown intermediate point.

In this figure, m is the tip mass, l is the length of the arm, $l_2 = \lambda l$, $0 < \lambda < 1$ is the location of the contacted intermediate point, F_{n} is the contact force (the reaction force of the surface on the link), F_{e} is the interaction force applied on the object, Γ_l is the coupling torque, θ_m is the motor angle, θ_t is the angular position of the tip mass (load angle), θ_c represents the angular position of the collision point, θ_e is the equilibrium angular position of the impact surface, and $c = \frac{3EI}{l}$ is the rotational stiffness coefficient of the arm, which is considered constant throughout the whole flexible structure as occurs in refs. [15, 19]. Next, the assumptions in ref. [34] and the following assumptions are considered:

- Assumption 1: There are no rebounds.
- Assumption 2: The collision point between the flexible arm and the environment occurs in an intermediate point of the link.
- Assumption 3: The contact force is defined by its normal component, that is, its component in the Y axis. Therefore, the tangential component is ignored.
- Assumption 4: The mechanical impedance of the environment is represented by the spring-damper system.
- Assumption 5: The stiffness parameter EI is constant throughout all of the beam.

Let us decompose the robot link into two segments, the first one from $x = 0$ to $x = l_2$ and the second one from $x = l_2$ to $x = l$. If the assumptions 4–8 and 11 hold, the deflection of each of these intervals is given by a third-order polynomial:

$$y_i(x) = q_{i,0} + q_{i,1}(x - l_i) + q_{i,2}(x - l_i)^2 + q_{i,3}(x - l_i)^3 \tag{1}$$

where $i = 1, 2$ is the ordinal of the segment, $q_{i,j}$ are the polynomial coefficients (which are different in each interval), $l_1 = 0$, and $l_2 = \lambda l$. The mechanical impedance of the environment is described by the well-known spring-damp system:

$$F_e = k_e(y(\lambda l) - y_e) + v_e \frac{d(y(\lambda l) - y_e)}{dt} \tag{2}$$

where k_e and v_e are the stiffness and damping characteristics of the environment, respectively, y_e is the equilibrium position of the impacted surface (its "y" coordinate in the X-Y frame), and $y(\lambda l)$ is the position of the point of the link that contacts the object. Substituting $y(\lambda l) = l_2\theta_c = \lambda l\theta_c$ and $y_e = l_2\theta_e = \lambda l\theta_e$ into (2) results:

$$F_e = k_e \lambda l(\theta_c - \theta_e) + v_e \lambda l \frac{d(\theta_c - \theta_e)}{dt} \tag{3}$$

Since y_e is a fixed point in the plane, we have therefore that $\frac{d(\theta_e)}{dt} = 0$ and the Eq. (3) is transformed as follows:

$$F_e = k_e \lambda l(\theta_c - \theta_e) + v_e \lambda l \frac{d(\theta_c)}{dt} \tag{4}$$

Equating rotational moments with respect to the axis Z yields:

$$\Gamma_l = ml^2 \ddot{\theta}_t - l_2 F_n = ml^2 \ddot{\theta}_t + k_e \lambda^2 l^2 (\theta_c - \theta_e) + v_e \lambda^2 l^2 \dot{\theta}_c \tag{5}$$

where it has been taken into account that $F_e = -F_n$. The equations of arm deflection are as follows:

$$\begin{aligned} y_1(x) &= q_{1,0} + q_{1,1}x + q_{1,2}x^2 + q_{1,3}x^3 \\ y_2(x) &= q_{2,0} + q_{2,1}(x - l_2) + q_{2,2}(x - l_2)^2 + q_{2,3}(x - l_2)^3 \end{aligned} \tag{6}$$

where the coefficients $q_{1,0}$, $q_{1,1}$, $q_{1,2}$, $q_{1,3}$, $q_{2,0}$, $q_{2,1}$, $q_{2,2}$, and $q_{2,3}$ are given by:

$$\begin{aligned} q_{1,0} &= q_{1,1} = 0 \\ q_{1,2} &= \frac{1}{2EI}\left(-ml^2\ddot{\theta}_t + \lambda l F_n\right) \\ q_{1,3} &= \frac{1}{6EI}\left(ml\ddot{\theta}_t - F_n\right) \\ q_{2,0} &= y_1(l_2) = \frac{ml^4\lambda^2(\lambda - 3)}{6EI}\ddot{\theta}_t + \frac{2l^3\lambda^3}{6EI}F_n \\ q_{2,1} &= \frac{dy_1(l_2)}{dt} = \frac{ml^3\lambda(\lambda - 2)}{2EI}\ddot{\theta}_t + \frac{l^2\lambda^2}{2EI}F_n \\ q_{2,2} &= -\frac{ml^2(1 - \lambda)}{2EI}\ddot{\theta}_t \\ q_{2,3} &= \frac{ml}{6EI}\ddot{\theta}_t \end{aligned} \tag{7}$$

On the one hand, the deviation of the contact point of the link of the flexible arm can be expressed as follows:

$$\begin{aligned} y_1(l_2) = l_2(\theta_c - \theta_m) &= q_{1,0} + q_{1,1}l_2 + q_{1,2}l_2^2 + q_{1,3}l_2^3 \\ &= \frac{l^2\lambda^2}{2EI}\left(-ml^2\ddot{\theta}_t + \lambda l F_n\right) + \frac{l^3\lambda^3}{6EI}\left(ml\ddot{\theta}_t - F_n\right) \end{aligned} \tag{8}$$

After simplifying, Eq. (8) can be rewritten as:

$$\frac{2c}{l}(\theta_c - \theta_m) = ml\lambda(\lambda - 3)\ddot{\theta}_t + 2\lambda^2 F_n \tag{9}$$

On the other hand, the deviation of the contact point at the end point of the flexible arm can be expressed as follows:

$$\begin{aligned} y_2(l) &= q_{2,0} + q_{2,1}(l - l_2) + q_{2,2}(l - l_2)^2 + q_{2,3}(l - l_2)^3 \\ &= \frac{ml^4\lambda^2(\lambda - 3)}{6EI}\ddot{\theta}_t + \frac{2l^3\lambda^3}{6EI}F_n + \left(\frac{ml^3\lambda(\lambda - 2)}{2EI}\ddot{\theta}_t + \frac{l^2\lambda^2}{2EI}F_n\right)l(1 - \lambda) \\ &\quad - \frac{ml^2(1 - \lambda)}{2EI}l^2(1 - \lambda)^2\ddot{\theta}_t + \frac{ml}{6EI}l^3(1 - \lambda)^3\ddot{\theta}_t \\ &= l(\theta_t - \theta_m) \end{aligned} \tag{10}$$

After simplifying, the following equation can be obtained:

$$\frac{2c}{l}\left(\theta_t - \theta_m\right) = -2ml\ddot{\theta}_t + \lambda^2\left(3-\lambda\right)F_n \tag{11}$$

Considering the system of Eqs. (9) and (11), the angular position of the end point of the beam (θ_t) and the angular position of the intermediate point of the beam which has contact with the environment (θ_c) can be obtained by solving this system of equations as follows:

$$X = M^{-1} \times N \tag{12}$$

Where X, M, and N can be expressed as the following equations:

$$\begin{aligned} X &= \begin{pmatrix} \ddot{\theta}_t \\ \dot{\theta}_c \end{pmatrix} \\ M &= \begin{pmatrix} ml\lambda\left(3-\lambda\right) & 2v_e\lambda^3 l \\ 2ml & \left(3-\lambda\right)v_e\lambda^3 l \end{pmatrix} \\ N &= \begin{pmatrix} \frac{2c}{l}\left(\theta_m - \theta_c\right) - 2k_e\lambda^3 l\left(\theta_c - \theta_e\right) \\ \frac{2c}{l}\left(\theta_m - \theta_t\right) - \left(3-\lambda\right)k_e\lambda^3 l\left(\theta_c - \theta_e\right) \end{pmatrix} \end{aligned} \tag{13}$$

Unlike the collision at the end point of the beam, in this case, the structure of dynamics model will not be integrated in the free and constrained motion mode. In the free motion mode, the dynamics model is described by two state variables. However, after collision at an intermediate point of the link, in the constrained motion mode, the dynamics model is described by three state variables. Therefore, the governing dynamical equations in the constrained motion mode can be obtained as Eq. (12). In the free motion mode, we assumed that the beam tip had hit the object with zero impedance. Thus, the governing dynamical equations of the beam tip are as follows:[19]

$$\begin{aligned} &F_n = 0 \\ &ml^2\ddot{\theta}_t = c\left(\theta_m - \theta_t\right) \\ &\Gamma_l = c\left(\theta_m - \theta_t\right) \end{aligned} \tag{14}$$

Next, the dynamics model of the single-link flexible arm is completed by introducing the actuator dynamics.

2.2. *Motor dynamics*

In this work, a DC motor with a reduction gear is used, which is a common electromechanical actuator used in many control systems in order to drive robotic links. This actuator is operated by a current servo-amplifier. The current servo-amplifier controls the input current to the motor which is proportional to the voltage supplied to the servo-amplifier by the computer. The block diagram of the actuator (servo-amplifier + motor + gear) is shown in Figure 2 whose equations are given by the following:

$$Motor: \quad \hat{k}_m\hat{i} = J\ddot{\hat{\theta}}_m + v\dot{\hat{\theta}}_m + \hat{\Gamma}_{F_m} + \hat{\Gamma}_l \tag{15}$$

$$Servo-amplifier: \quad \hat{i} = \hat{k}_a u \tag{16}$$

$$Gear: \quad \hat{\theta}_m = \hat{\theta}_l n; \qquad \hat{\Gamma}_l = \frac{\Gamma_l}{n}; \qquad \hat{\Gamma}_{F_m} = \frac{\Gamma_{F_m}}{n} \tag{17}$$

where $\hat{k}_m$ is the electromechanical constant of the motor, $\hat{i}$ is the current supplied to the motor by the servo-amplifier, $\hat{J}$ is the motor inertia, $\hat{v}$ is the viscous friction of the motor, $\hat{\Gamma}_{F_m}$ is the unknown Coulomb friction torque, $\hat{\Gamma}_l$ is the coupling torque between the flexible slewing link and the motor shaft, u is the voltage supplied to the servo-amplifier generated by the computer, $\hat{k}_a$ is the servo-amplifier gain, n is the reduction ratio of the gear, $\hat{\theta}_m$ is the motor angle, and θ_m is the load angle

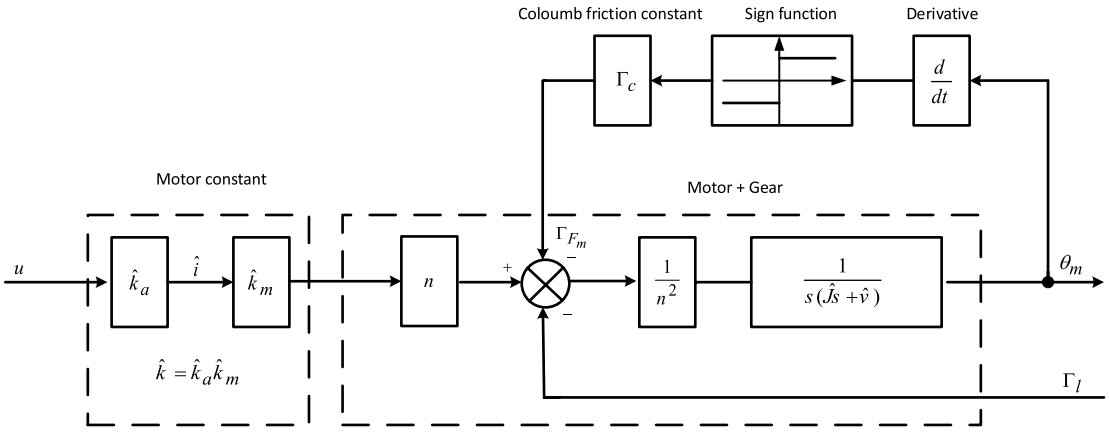

Fig. 2. Block diagram of the actuator.

(or the motor angle in the gear outlet). Variables and parameters with upper hat are referred to the motor side of the gear. For example, the conversion between angles of the motor is $\hat{\theta}_m = \theta_m n$ and the conversion between the torques is $\hat{\Gamma}_l = \frac{\Gamma_l}{n}$. Therefore, by combining the above Eq. (15)–(17), the complete actuator system dynamics is obtained by the following equation:

$$knu = \hat{J}n^2\ddot{\theta}_l + \hat{v}n^2\dot{\theta}_l + \Gamma_{F_m} + \Gamma_l \tag{18}$$

where $k = k_m k_a$. The Coulomb friction is considered as a perturbation which affects the system dynamics. This perturbation depends on the sign of the motor angular velocity. Therefore, the model of the Coulomb friction torque can be defined by the following equation:

$$\Gamma_{F_m} = \begin{cases} \Gamma_c.sign(\dot{\theta}_m) & \dot{\theta}_m \neq 0 \\ sign(u).\min(k\,|nu|\,,\Gamma_c), & \dot{\theta}_m = 0 \end{cases} \tag{19}$$

where Γ_c is an unknown constant value which is different for each motor and represents the static friction value which the motor torque must exceed to begin the movement, also called the Coulomb friction coefficient. The first case shows the Coulomb friction torque when the motor is moving, and the second case shows the same torque when the motor is stopped.

3. Controller Design

In this section, an adaptive robust control system is designed for the impedance control of the single-link flexible arm which is valid for both free and constrained motions. Figure 3 illustrates the closed-loop control system scheme in which Block I demonstrates the linear plant analyzed in the previous section for constrained motions (servo-amplifier + DC gear motor + arm + environment), Block III estimates the contact length ($l_2 = \lambda l$), determines the contact angle (θ_c), and calculates the contact force which is exerted to the environment (F_e), and Block II and Block IV represent the robust impedance control based on the position control with force tracking in which the position control (Block IV) is an adaptive PID controller based on sliding mode control. Figures 4 and 5 detail the block I and the block III, respectively.

In the case in which the collision between the link and the environment happened at an intermediate point of the link, it is assumed that the environment parameters are known. Instead, the collision point is unknown (the parameter λ is uncertain). For determining the contact force and the angular position of the impact point, a fictitious arm is considered that moves simultaneously with the real arm and hits the environment at a known intermediate point. It should be reminded that the impact point with the environment can be changed at the fictitious arm length. The fictitious arm is stimulated by the measured position of the motor (θ_m). Before we design the controller, it should be considered that the model must be valid for both constrained and free movements. Therefore, we utilize the linear dynamic model (12) for constrained motion mode with collision at the intermediate points and utilize the linear dynamic model (14) in free motion mode. In the free motion mode, it is assumed that the end-effector in the zero initial contact angle had hit the object with zero impedance.

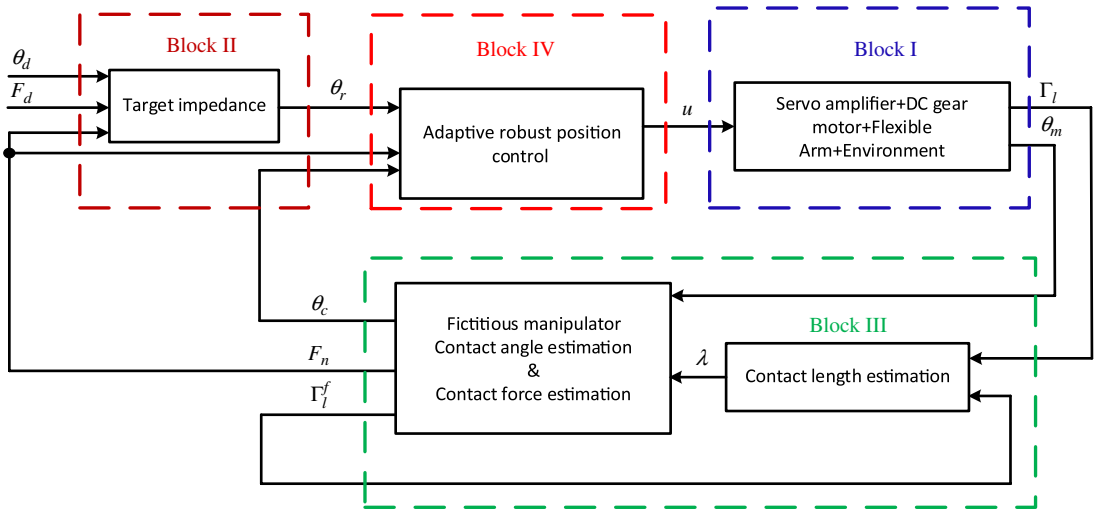

Fig. 3. Closed-loop control system scheme.

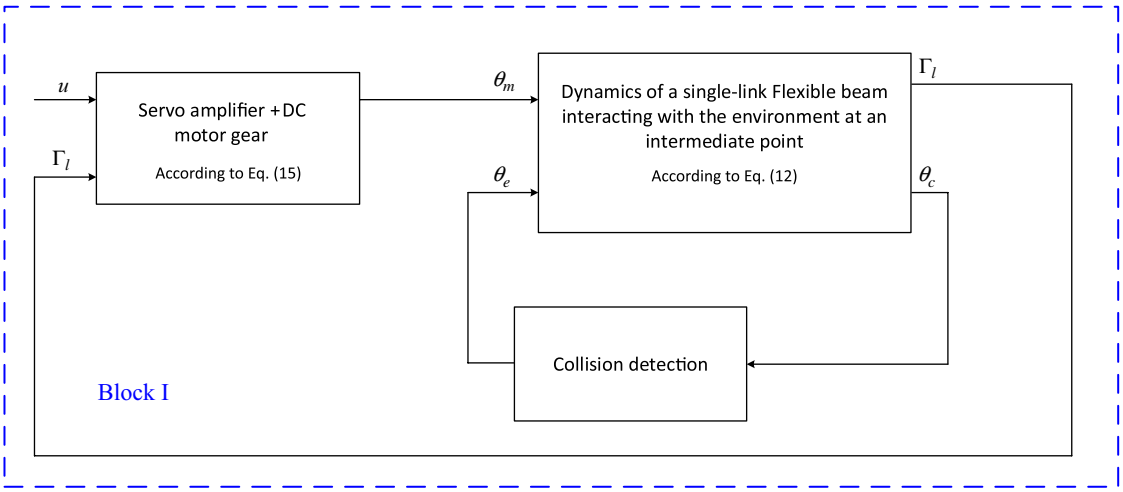

Fig. 4. Dynamics model of actuator, flexible-link and environment.

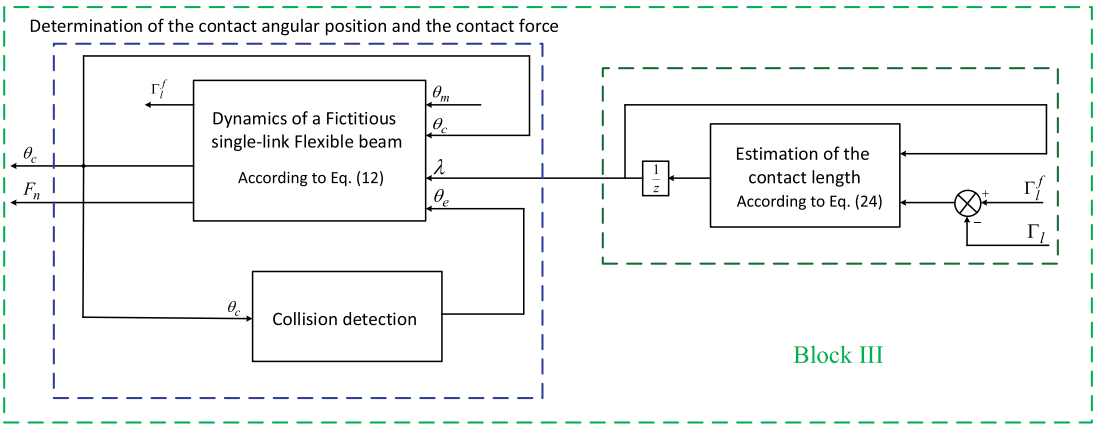

Fig. 5. Estimation of the contact length and determination of the contact angle and the contact force.

After determining the unified model that is able to represent the dynamic characteristics of the flexible link in both constrained and free motion modes, the unified controller is designed with only one parameter set which satisfies the control task requirements. As mentioned in the Introduction, in the free motion, the applied force to the environment is zero and the reference trajectory for the position control block is the desired trajectory (θ_d). In the constrained motion, the reference trajectory for the position is determined by the desired impedance dynamic which is generated by the target impedance block in Figure 3 (θ_r). Assuming that the position controller is accurate and assuming the dynamics and the geometry of the environment are known, the stiffness gain of the desired impedance could be selected so that the contact force could be regulated to the desired value. Therefore, the precise design of the position controller is the main part of this work in the robust impedance control. In the following, the task of the Block II, Block III, and Block IV will be explained.

3.1. Adaptive robust impedance control scheme with force regulation at the intermediate point of the link (Block II)

Consider the target impedance equation, which combines the position and the interaction force as the following equation:

$$F_e = k_m \left(\ddot{\theta}_d - \ddot{\theta}_r\right) + k_d \left(\dot{\theta}_d - \dot{\theta}_r\right) + k_p \left(\theta_d - \theta_r\right) \tag{20}$$

where θ_d and θ_r represent the desired angle and the reference angle for the position controller, respectively. F_e is the reaction force of the surface on the link which is obtained from (4). Moreover, k_m, k_d, and k_p are target parameters for the desired impedance. In the steady state, by assuming the accurate position control and regulating the contact force to a desired value, the two Eqs. (20) and (11) are re-written as follows:

$$F_d = k_p \left(\theta_d - \theta_c\right) \tag{21}$$

$$F_d = k_e \lambda l \left(\theta_c - \theta_e\right) \tag{22}$$

In Eq. (21), k_p is the impedance gain corresponding to the information of the motionless object to regulate the interaction force to the desired value (F_d). Therefore, using Eqs. (21) and (22), the impedance stiffness coefficient could be selected such that the interaction force applied on the object is regulated to the desired value as the following equation:

$$k_p = \frac{F_d k_e \lambda l}{k_e \lambda l \left(\theta_d - \theta_e\right) - F_d} \tag{23}$$

3.2. Estimation of the contact length and calculation of contact angle and contact force (Block III)

In this section, we use a fictitious arm to estimate the contact length. In this way, the fictitious arm is stimulated at the same time that the real arm is stimulated by the motor angle of the real arm. Therefore, the exact angular position of the collision point at the real arm's length is determined by updating the parameter λ according to the following updated equation:

$$\lambda_{new} = \lambda_{old} + \alpha \left(\Gamma_l^f - \Gamma_l\right) \tag{24}$$

Where α represents a learning rate, Γ_l^f is the coupling torque of the fictitious arm, and Γ_l is the measured coupling torque of the real arm. It should be noted that both of the arms (real and fictitious arms) are stimulated by the motor angle of the real arm. Therefore, by choosing an appropriate value for the α and by starting from an initial value of λ, the contact length of the impact point converges to its actual value (see convergence proof of the algorithm in Appendix A). Thus, by specifying the contact length ($l_2 = \lambda l$), the information needed for the impedance controller is obtained by using the governing dynamical equations.

3.3. Adaptive robust position-based impedance control scheme (Block IV)

As aforementioned, the main part of the impedance control design in this work is related to the design of the position control. Eliminating the deflection caused by the link flexibility is the significant challenge of the position control in the flexible link. To solve this challenge, one may consider the flexible

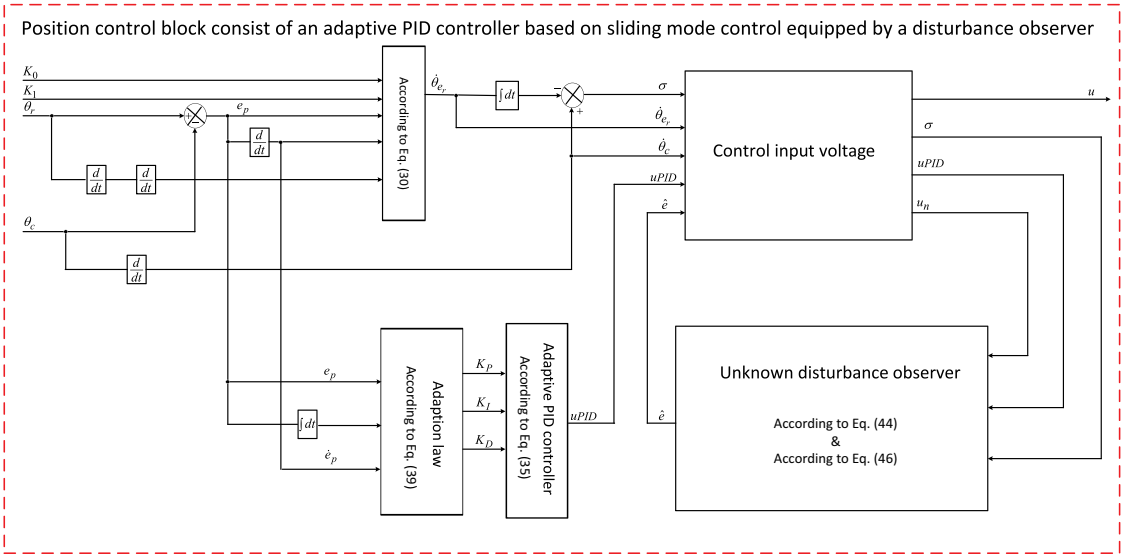

Fig. 6. Position control block consist of an adaptive PID controller based on sliding mode control equipped by a disturbance observer.

link as a rigid one by assuming that the deflection of the flexibility is caused by an input disturbance. The undesirable effect of deflection must somehow be eliminated. Therefore, the proposed adaptive sliding mode controller is equipped by a disturbance observer in order to remove this adverse effect. In the next subsection, the PID adaptive controller based on sliding mode control is described which is equipped by a disturbance observer. Figure 6 details the position control strategy (Block IV) consisting of the PID adaptive controller based on the sliding mode controller. As can be seen from this figure, the adaptive PID sliding mode control (APIDSMC) is equipped by a disturbance observer.

3.3.1. Adaptive controller equipped by a disturbance observer. The interaction force applied on the environment is given by Eq. (4). Thus, Eq. (5) can be rewritten as:

$$\Gamma_l = ml^2 \Delta\ddot{\theta}_c + F_e l_2 \tag{25}$$

A gain, we consider Eq. (18), which is related to the dynamics of actuator system as follows:

$$knu = \hat{J}n^2\ddot{\theta}_l + \hat{v}n^2\dot{\theta}_l + \Gamma_{F_m} + \Gamma_l \tag{26}$$

In this study, the main idea in the position control of the flexible link is based on this assumption that the deflection of the beam tip can be considered as a disturbance in the control input. Thus, according to this hypothesis, the contact angle of the beam (θ_c) is considered as equal as the motor angle (θ_l). Instead, the source of the beam deflection is considered in the voltage input. Therefore, the governing dynamical equation of the flexible link with the motor dynamics becomes a second-order equation which in the state-space representation can be expressed as follows:

$$\begin{cases} \dot{x}_1(t) = x_2(t) \\ \dot{x}_2(t) = ax_2(t) + b\,(u(t) + V_d(\mathrm{t})) + z + \Gamma^d_{F_m} \end{cases} \tag{27}$$

where, $x_1(t) = \Delta\theta_c(t)$, $x_2(t) = \Delta\dot{\theta}_c(t)$, $a = -\frac{vn^2}{Jn^2+ml^2}$, $b = \frac{Kn}{Jn^2+ml^2}$, and $\mathrm{z} = -\frac{F_e l}{Jn^2+ml^2}$. $\Gamma^d_{F_m}$ is the unknown Coulomb friction disturbances, $u(t)$ and $V_d(\mathrm{t})$ represent the control signal (control input voltage) and the input disturbance, respectively. In the sliding mode control theory, an appropriate sliding surface is selected and the control input is, then, designed such that the sliding surface satisfies the sliding sufficient condition. This makes the system robust against uncertainties such as parameter variations, frictions, and disturbances. In the following, $e\,(x,\,t)$ represents the unknown disturbance

term which is defined as:

$$e\,(x,\,t) = bV_{\mathrm{d}} + \Gamma_{F_m}^{d} \tag{28}$$

We define the error between the command angular position trajectory θ_r and the contact angular position as follows:

$$e_p = \theta_r - \theta_c \tag{29}$$

In order to achieve a second-order error dynamics, the signal is defined as follows:

$$\dot{\theta}_{er} = \ddot{\theta}_r + K_1\dot{e}_p + K_0 e_p \tag{30}$$

where K_1 and K_0 are chosen by designers such that roots of $s^2 + K_1 s + K_0 = 0$ are in the open left-half complex plane. In general, we can choose $\mathrm{K}_1 = 2\xi\omega_{\mathrm{n}}$ and $\mathrm{K}_1 0 = \omega_n^2$, where ξ is the damping ratio and ω_{n} is the natural frequency. A typical sliding surface can be selected as:

$$\sigma = \dot{\theta}_c - \theta_{er} \tag{31}$$

If sliding mode occurs, that is, $\sigma = 0$, then

$$\dot{\theta}_c = \theta_{er} \tag{32}$$

Substituting (32) into (30) yields:

$$\ddot{e}_p + K_1\dot{e}_p + K_0 e_p = 0 \tag{33}$$

This implies that error will tend to zero ($e_p \to 0$) as time goes to infinity ($t \to \infty$). Next, the control input u which must be designed is split into three parts, namely, u_{PID}, u_s, and u_n as follows:

$$u = u_{PID} + u_s + u_n \tag{34}$$

with

$$u_{PID} = \frac{1}{b}\left(K_P e_p + K_I \int e_p dt + K_D \dot{e}_p\right) \tag{35}$$

$$u_s = -\frac{1}{b}\left(ax_2 + z - \left|\dot{\theta}_{er}\right| + k_s\sigma + k_{st}\mathrm{sat}\,(\sigma)\right) \tag{36}$$

$$\mathrm{sat}\,(\sigma) = \begin{cases} sgn\sigma & if\ |\sigma| > \varphi \\ \frac{\sigma}{\varphi} & if\ |\sigma| < \varphi \end{cases} \tag{37}$$

$$u_n = -\frac{1}{b}\hat{e} \tag{38}$$

where k_s, k_{st}, and φ are adjustable positive constants. The component u_n is used to compensate the unknown disturbance e. The discontinuous sentence u_s with its smooth approximation is used to reduce the chattering phenomenon at the reaching phase in the sliding mode control and is also used to compensate the known terms. The three PID controller gains, K_P, K_I, and K_D, can be updated by a proper gradient-based adaptation mechanism to provide a robust controller as the following equations:

$$\begin{aligned} \dot{K}_P &= -\eta_1\sigma e_p(t) \\ \dot{K}_I &= -\eta_2\sigma \int_0^t e_p(\tau)d\tau \\ \dot{K}_D &= -\eta_3\sigma \frac{d}{dt}e_p(t) \end{aligned} \tag{39}$$

where, $\eta_i > 0$, $i = 1, 2, 3$ is the learning rate. It should be noted that the η_i $i = 1, 2, 3$, K_P, K_I, and K_D should be carefully chosen such that lead to guarantee the stability and the convergence of system. In order to prove the controller stability, let the Lyapunov function be considered as follows:

$$V_c = \frac{1}{2}\left(\sigma^2 + \frac{1}{\eta_1}K_P^2 + \frac{1}{\eta_2}K_I^2 + \frac{1}{\eta_3}K_D^2\right) \tag{40}$$

Taking derivative both sides of (40) yields,

$$\dot{V}_c = \sigma\dot{\sigma} + \frac{1}{\eta_1}K_P\dot{K}_P + \frac{1}{\eta_2}K_I\dot{K}_I + \frac{1}{\eta_3}K_I\dot{K}_I \tag{41}$$

Substituting adaptive laws (39) into (41) and simplifying, then (41) can be rewritten as:

$$\dot{V}_c = -k_s\sigma^2 - k_{st}\text{sat}(\sigma)\,\sigma + \tilde{e} \tag{42}$$

In (42), $\tilde{e} = e - \hat{e}$ is the disturbance estimation error. If the disturbance estimation ($\hat{e}$) is such that the estimation error ($\tilde{e}$) goes close to zero, the $\dot{V}$ will be negative semi-definite, thereby the stability of controller is guaranteed. Therefore, the control law given by (34) and adaptive laws (39) guarantee the reaching and sustaining of the sliding mode. Thus, in spite of the link deflection, the reference trajectory which is generated by the target impedance block will be tracked. In the next subsections, a disturbance observer is proposed to estimate the unknown disturbance (e).

3.3.2. Disturbance observer. In this section, a disturbance observer is designed to estimate e such that the estimation error $\tilde{e}$ tends to zero. The disturbance observer is a modified version of that presented in ref. [40]. Let the estimate of the uncertainty e be expressed by the following equation:

$$\hat{e} = \hat{d}(t) + p(\sigma) \tag{43}$$

where $\hat{d}(t)$ and $\hat{e}$ are an update law which can be considered as the internal state of the observer and the estimate of the unknown disturbance, respectively, and $p(\sigma)$ may be a linear or nonlinear scalar function of σ. The $\hat{d}(t)$ should be selected in such a way that the $\hat{e}$ approaches e and thereby the estimate error goes to zero. Taking derivative from both sides of Eq. (43) and substituting $\dot{\sigma}$ obtains:

$$\dot{\hat{e}} = \dot{\hat{d}}(t) + \frac{\partial p}{\partial \sigma}\left(-k_s\sigma - k_{st}\text{sat}(\sigma) + b\left(u_{PID} + u_n\right) + e\right) \tag{44}$$

The dynamics of $\hat{d}(t)$ is considered as follows:

$$\dot{\hat{d}}(t) = -\frac{\partial p}{\partial \sigma}\left(-k_s\sigma - k_{st}\text{sat}(\sigma) + \hat{e} + b\left(u_{PID} + u_n\right)\right) \tag{45}$$

Therefore, the dynamics of $\hat{e}$ can be obtained as:

$$\dot{\hat{e}} = \frac{\partial p}{\partial \sigma}\tilde{e} \tag{46}$$

Subtracting both sides of (46) from $\dot{e}$ results:

$$\dot{\tilde{e}} = -\frac{\partial p}{\partial \sigma}\tilde{e} + \dot{e} \tag{47}$$

For the stability of $\tilde{e}$, $p(\sigma)$ must be chosen such that $\frac{\partial p}{\partial \sigma}$ be a positive function and the derivative of e to be bounded as follows:

$$|\dot{e}| < \mu \tag{48}$$

where μ represents a positive number. In the following section, the stability analysis of closed-loop system and the boundedness of $\tilde{e}$ and σ will be explained.

4. Stability Analysis of Closed-Loop Control System

In this section, the stability condition of closed-loop control system was taken from ref. [42]. For stability analysis, a candidate Lyapunov function is considered as follows:

$$\begin{aligned} V(\sigma, \tilde{e}) &= V_c + \frac{1}{2}\tilde{e}^2 \\ &= \frac{1}{2}\left(\sigma^2 + \tilde{e}^2 + \frac{1}{\eta_1}K_P^2 + \frac{1}{\eta_2}K_I^2 + \frac{1}{\eta_3}K_D^2\right) \end{aligned} \tag{49}$$

Taking the time derivative from both sides of (49) and using (42) and (48) obtains:

$$\begin{aligned}\dot{V}(\sigma,\tilde{e}) &= \sigma\dot{\sigma} + \dot{\tilde{e}}\tilde{e} + \tfrac{1}{\eta_1}K_P\dot{K}_P + \tfrac{1}{\eta_2}K_I\dot{K}_I + \tfrac{1}{\eta_3}K_D\dot{K}_D \\ &= -k_s\sigma^2 - k_{st}sat(\sigma)\,\sigma + \tilde{e}\sigma + \tilde{e}\dot{e} - \tfrac{\partial p}{\partial\sigma}\tilde{e}^2\end{aligned} \tag{50}$$

Using Young's inequality, $ab \le \frac{1}{2}\left(a^2+b^2\right)$, and (48), Eq. (50) can be rewritten as:

$$\dot{V}(\sigma,\tilde{e}) \le -\left(k_s - \frac{1}{2}\right)\sigma^2 - \left(\frac{\partial p}{\partial\sigma} - 1\right)\tilde{e}^2 + \frac{1}{2}\mu^2 - k_{st}\,sat(\sigma)\,\sigma \tag{51}$$

The control parameter can be chosen such that $\left(k_s - \frac{1}{2}\right)$ and $\left(\frac{\partial p}{\partial\sigma} - 1\right)$ are always positive. From (51), it can be proved that the dynamics of σ and the uncertainty estimation error $\tilde{e}$ are not asymptotically stable but ultimately bounded.[41] The upper bounds of $|\tilde{e}|$ and $|\sigma|$ can be obtained from (52) and (53), respectively.

$$|\tilde{e}| \le \gamma = \frac{\mu}{\sqrt{2\left(\frac{\partial p}{\partial\sigma} - 1\right)}} \tag{52}$$

$$|\sigma| \le \frac{\gamma + \sqrt{\gamma^2 + 4k_s\mu\gamma}}{2k_s} \tag{53}$$

Therefore, from (52) and (53), the uncertainty estimation error $\tilde{e}$ and σ are ultimately bounded and the control parameter such as $\frac{\partial p}{\partial\sigma}$, k_s, and k_{st} can be chosen so that the bounds on $|\tilde{e}|$ and $|\sigma|$ can be made sufficiently small.

5. Performance Criteria

In this section, the following performance criteria are defined in order to evaluate the performance of the controller:

- Root-mean-squared error (RMSE) for the trajectrory tracking in the constrained and free motion phase.

$$RMSE = e_p + e_f \tag{54}$$

where $e_p = \sqrt{\sum_{t=0}^{t_c} \|\theta_d(t) - \theta_t(t)\|^2\, T/t_f}$ and $e_f = \sqrt{\sum_{t=tp}^{t_f} \|F_d(t) - F_e(t)\|^2\, T/t_f}$ represent the error value in the free motion and in the constrained motion mode, respectively.

- Root-mean-square value (RMSV) of the control input voltage .

$$RMSV = \sqrt{\sum_{0}^{t_f} \|u(t)\|^2\, T/t_f} \tag{55}$$

Both RMSE and RMSV are used as objective numerical measures of tracking performance for an entire error curve, where T is the sample time, t_c is the collision time, t_f and $t_p \in \left(t_c, t_f\right)$ represent the total running time of the simulations and a definite time in the collision phase, respectively. In our simulation, these parameters are chosen as, $T = 1 \cdot 10^{-3}$ s, $t_c = 3$ s, $t_f = 10$ s, and $t_p = 4.5$ s. The criterion RMSV shows the consumption of energy.

6. Computer Simulation Results

6.1. Computer simulation results in both constrained and unconstrained motion modes

System numerical simulations are performed using Simulink/MATLAB R2014a. The physical parameters of the system are shown in Table I which includes the flexible-link parameters, the motor

Table I. Physical parameters of the system.

Parameter	Description	Value
Data of the flexible arm		
E	Young modulus	271×10^9 Pa
I	Cross section inertia	3.017×10^{-12} m^4
ρ	Density	1800 kg/m^3
l	Length	0.98 m
d	Diameter	2.8×10^{-3} mm
m	Tip mass	43.71×10^{-3} kg
ξ_l	Friction coefficient	0.0458
c	Rotational stiffness	2.51
Data of the motor-gear set		
J	Total motor inertia+ reduction gear	6.87×10^{-5} kg m^2
v	Viscous friction	1.041×10^{-3} kg m^2/s
n	Reduction ratio of the motor gear	50
K	Motor constant	2.1×10^{-1} $\frac{\text{Nm}}{\text{V}}$
V_{sat}	Saturation voltage of the servo amplifier	± 10 V
Data of the environment		
k_e	Stiffness	$100 \frac{\text{N}}{\text{m}}$
v_e	Damping coefficient	$1 \frac{\text{Ns}}{\text{m}}$

Table II. Control parameters of the closed loop control system.

Parameter	Description	Value
Characteristics of the target impedance		
k_p	Target stiffness	k_p^*
k_d	Target damping coefficient	$\frac{k_p^*}{3}$
k_m	Target inertia coefficient	$\frac{k_p^*}{100}$
Characteristics of APIDSMC equiped by DO		
k_0	Control parameter	2
k_1	Control parameter	2.5
$K_P(0)$	Proportional gain initial value of the APID controller	1
$K_I(0)$	Integral gain initial value of the APID controller	1
$K_D(0)$	Derivative gain initial value of the APID controller	1
η_1	Learning rate of proportional gain term in adaption law	6.6
η_2	Learning rate of integral gain term in adaption law	0.001
η_3	Learning rate of derivative gain term in adaption law	0.5
k_s	Control parameter in the feedback control	0.1
k_{st}	Switching gain in the feedback control	0.1
$\frac{\partial p}{\partial \sigma}$	Control parameter in both free and constrained motion modes	4.5

parameters, and the environment parameters. Table II shows the system control parameters which includes the target impedance parameters and the proposed APIDSMC control strategy parameters.

In the following, the simulation has been carried out for constrained and unconstrained motion, in the presence of the unknown Coulomb friction disturbances. In the constrained phase, the desired contact force has been chosen equal to 20 N ($F_d = 20$ N) and in the unconstrained phase, the desired trajectory has been defined as the following equation:

$$\theta_d(t) = \begin{cases} 5t^2; & 0 \le t < 1 \\ 10t - 5; & 1 \le t < 3 \\ 10\left(4t - \frac{t^2}{2}\right) - 50; & 3 \le t < 4 \\ 30; & t \ge 4 \end{cases} \tag{56}$$

The simulation results are provided for the APIDSMC controller used in the position control scheme.

6.1.1. Simulation results for the APIDSMC controller with collision at the contact point length $\lambda = 0.7$ *and* $\lambda = 0.8$. In this section, the simulation has been carried out for $\lambda = 0.7$ and $\lambda = 0.8$. Figure 7 illustrates the simulation results for both constrained and unconstrained motion mode. Figure 7(a) shows the desired trajectory tracking in the free motion mode (position control). Figure 7(b) depicts the transient response of the desired contact force regulating in the constrained motion mode (force control). Figure 7(c) shows the coupling torque applied to the arm. Figure 7(d) illustrates the sliding surface at the reaching phase in the sliding mode control. Figure 7(e) shows the control input voltage to the DC motor.

As can be seen in Figures 7(a) and (b), before the contact ($t < 3$ s), in free motion mode, the contact point is equal to the tip angle. Therefore, the tip angular position follows the desired trajectory, and the contact force is zero. In this case, the system is controlled in free motion mode and the impedance controller acts as a position controller until the collision with the environment is detected at time $t = 3$ s. After the impact detection, the system firstly estimate the contact point length and then the contact point is used for the controller. Therefore, the system is controlled in constrained motion mode (during the contact ($t > 3$ s)). In this situation, the impedance controller acts as a regulating force controller and the controller immediately stabilises the system to track the reference trajectory (desired contact force) with null steady-state error. As shown in Figure 7(e), the control effort is very small and never saturates the amplifier which supplies the motor at 10 and -10 V, providing a smooth trajectory tracking without overheating the electrical system. The estimation of the contact point length and the convergence of the control parameters of the PID controller are shown in Figures 8 and 9, respectively.

6.2. Effects of environment parameters variations upon the system response in the constrained motion mode

In this work, it is assumed that the dynamics parameters of the environment are known. However, measuring these parameters in practice is always accompanied by error. Therefore, to investigate the robustness of the algorithm to variations of the environment parameters, a change of 10% was made in the environment parameters. The other remaining parameters of the system have been assumed unchanged. Simulation was performed for $\lambda = 0.8$, and the desired forces of 15, 20, and 25 Newton. In all three cases, the variation of 10% in the environment parameters (stiffness and damping coefficient) leads to a maximum of 1.14% error rate in the accuracy of force regulating. Figure 10 shows the simulation results for 10% variation in the environment parameters values (stiffness and damping coefficient) for regulating the contact force to the 20 Newton as a desired force.

6.3. Effects of link weight variations upon the system response in the constrained motion mode

In this section, effects caused in the system response because of changes in link weight (m) have been investigated. This payload variations can be occurred, for instance, due to the use of various tools placed at the end-effector of the manipulator. A range of possible payload values ($m_n \pm 0.5\, m_n$, $m_n = 0.044$ kg being the nominal value) have been chosen so that the arm could support under normal operating condition. The other remaining parameters of the system have been assumed unchanged. Therefore, there is no uncertainty in these parameters. Figure 11 shows the simulation results when the link weight parameter changes in the defined range.

As it can be observed from Figure 11, in the free motion mode, the maximum deviation of the system response with respect to the nominal case (m_n) is almost 0.7°, when m is equal to $m_{\min} = m_n - 0.5m_n$. In the constrained motion mode, the steady-state error of the desired contact force regulating is zero.

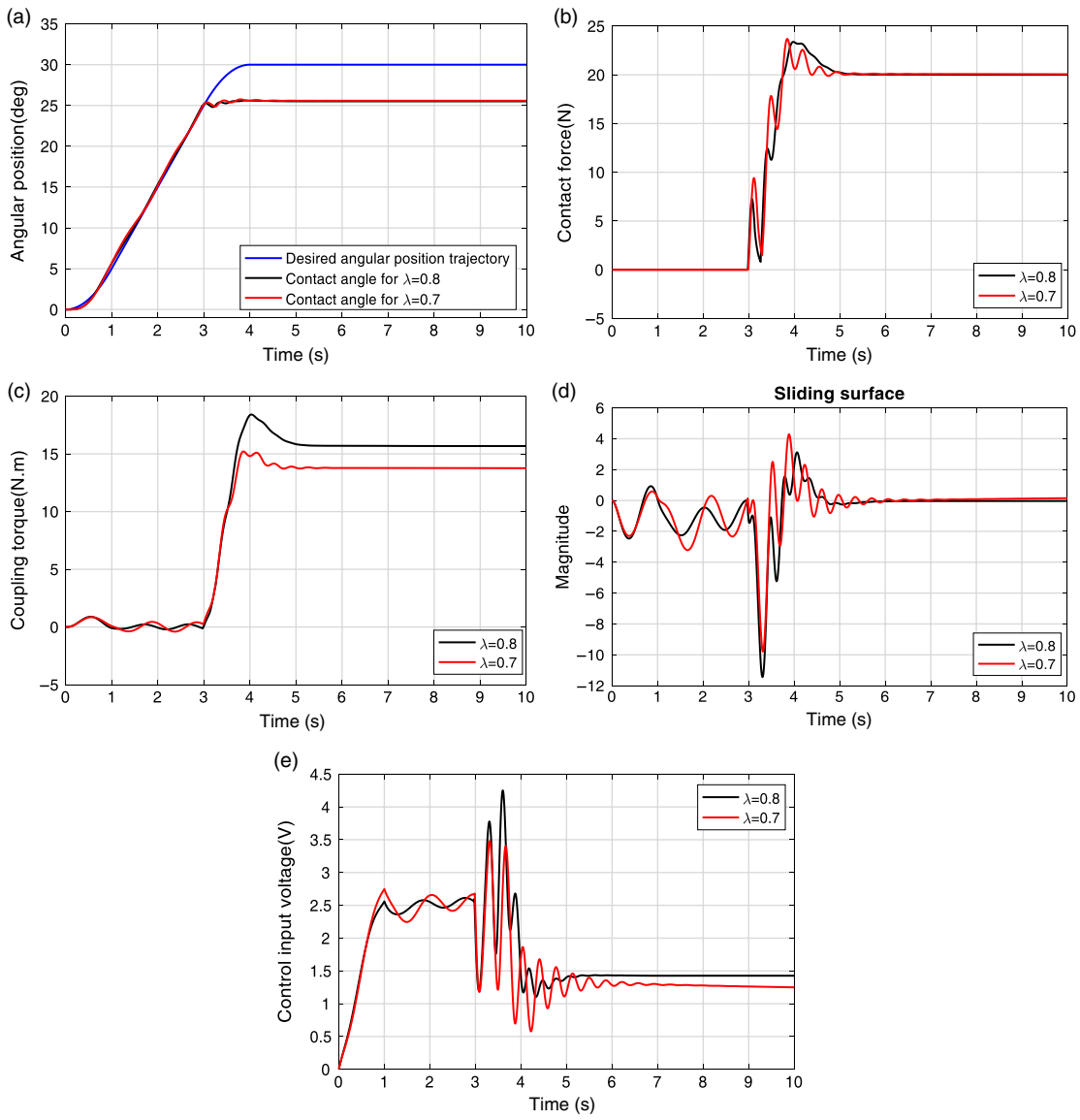

Fig. 7. System transient response in both free and constrained motion modes. (a) tracking of the prescribed desired trajectory (position control), (b) regulating the contact force to the desired value (force control), (c) coupling torque, (d) sliding surface, and (e) control input voltage.

Next, some simulation results are presented for simultaneous variations in the parameters of the DC motor.

6.4. Effects of inertia and viscous friction variations upon the system response

Viscous friction and inertia parameters of the DC motor only affect on the system in free motion mode in which there is a movement. Thus, by changing these parameters, the contact force profile in the steady state will remain intact. Therefore, in order to investigate the robustness of the proposed control method against the variations of the motor parameters, a change of 20% was made in these parameters (v and J). The other remaining parameters of the system have been assumed unchanged. Figure 12 illustrates the simulation results when the motor parameters change in the defined range.

As it can be observed from Figure 12, in the free motion mode, the maximum deviation of the system response with respect to the nominal case (J_n, v_n) is 0.8°, when J is equal to $J_{max} = J_n + 0.2J_n$ and v is equal to $v_{max} = v_n + 0.2v_n$. In the constrained motion mode, the steady-state error of the desired contact force regulating is zero. Next, some simulation results are presented for simultaneous variations in the weight of the link and in the viscous friction of the DC motor.

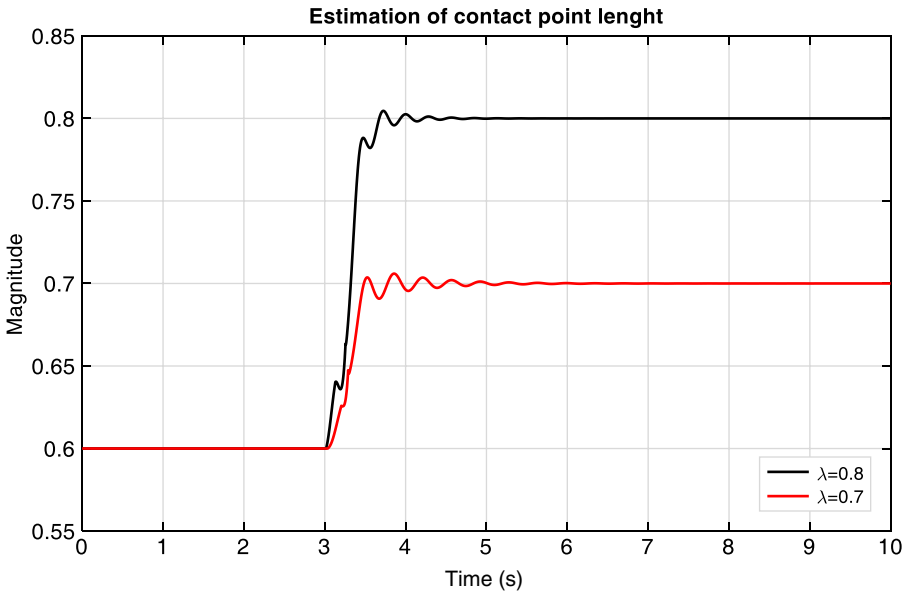

Fig. 8. Estimation of the contact point lenght.

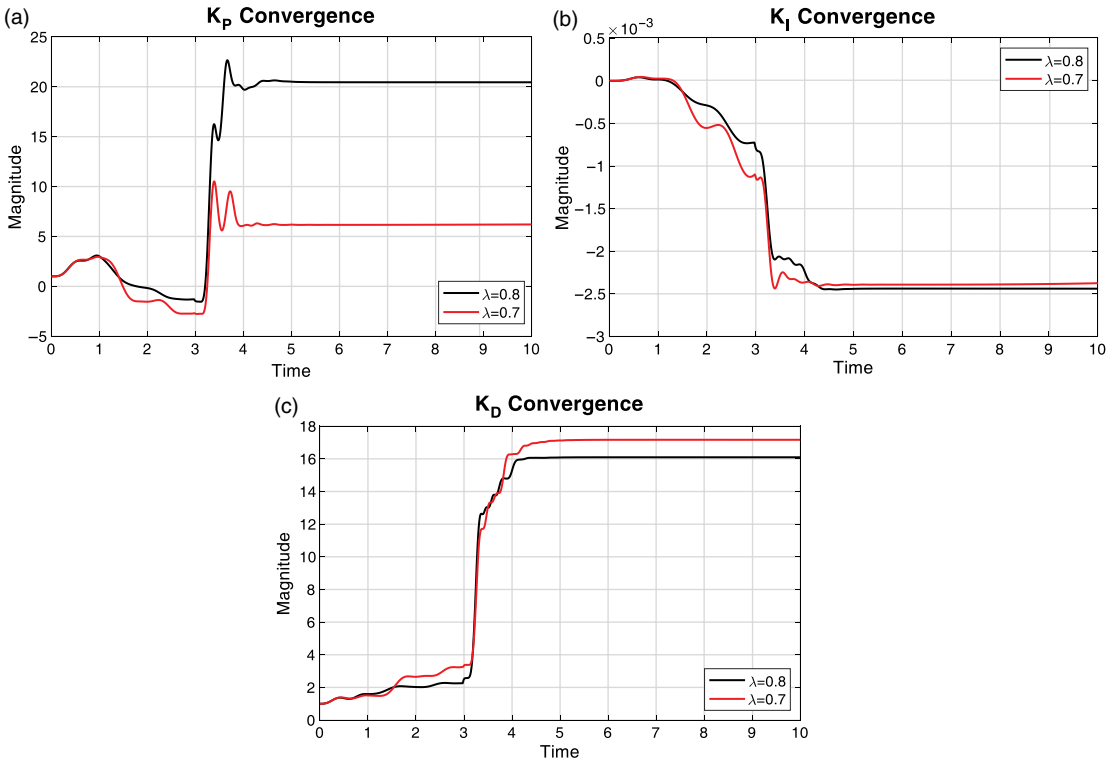

Fig. 9. Convegence of the PID controller. (a) K_P Convergence, (b) K_I Convergence. (c) K_D Convergence

6.5. Effects of payload and viscous friction variations upon the system response

In this section, effects caused in the system response because of changes in payload (m) and viscous friction (v) have been investigated. This payload variations can be occurred, for instance, due to the use of various tools placed at the end-effector of the manipulator. A range of possible payload values ($m_n \pm 0.25m_n$, $m_n = 0.044$ kg being the nominal value) have been chosen so that the arm could support under normal operating condition. The control system has also been studied under variations in the viscous friction parameter ($v_n \pm 0.1v_n$). The other remaining parameters of the system have been assumed unchanged. Therefore, there is no uncertainty in these parameters. Figure 13 shows the simulation results when both parameters vary at the same time in the defined range.

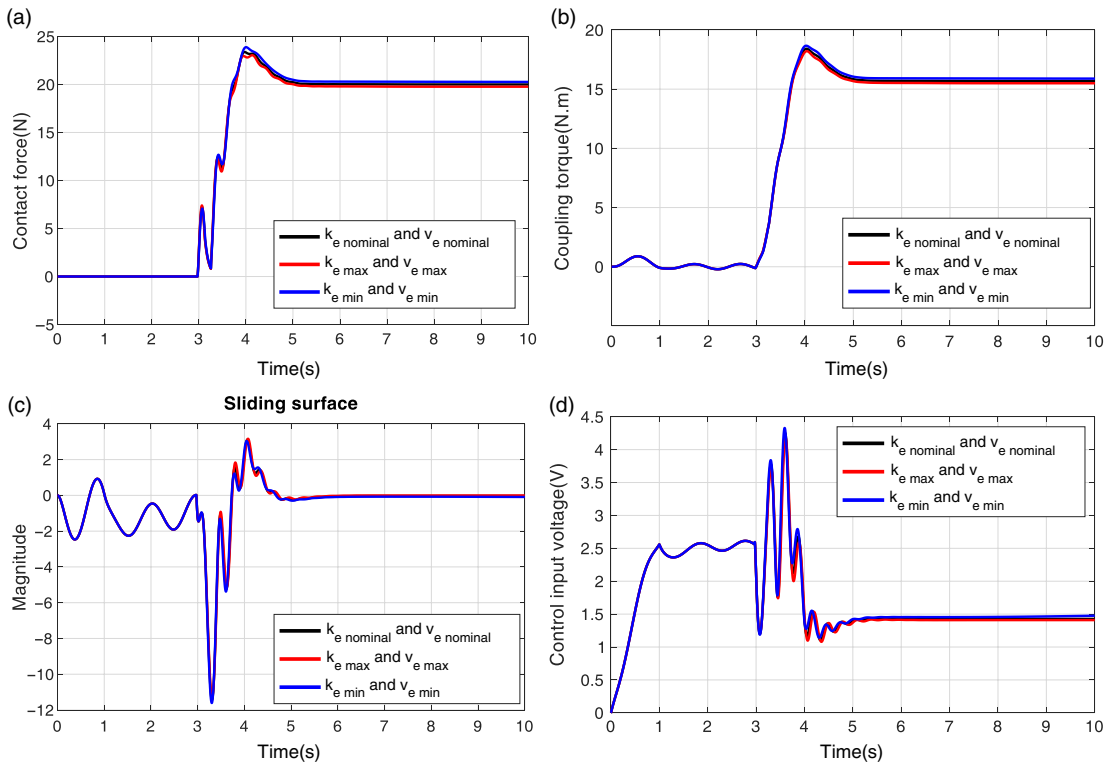

Fig. 10. System transient response in the constrained motion mode with 10 percent variation in the environment parameters values. (a) regulating the contact force to the desired value (force control), (b) coupling torque, (c) sliding surface, and (d) control input voltage.

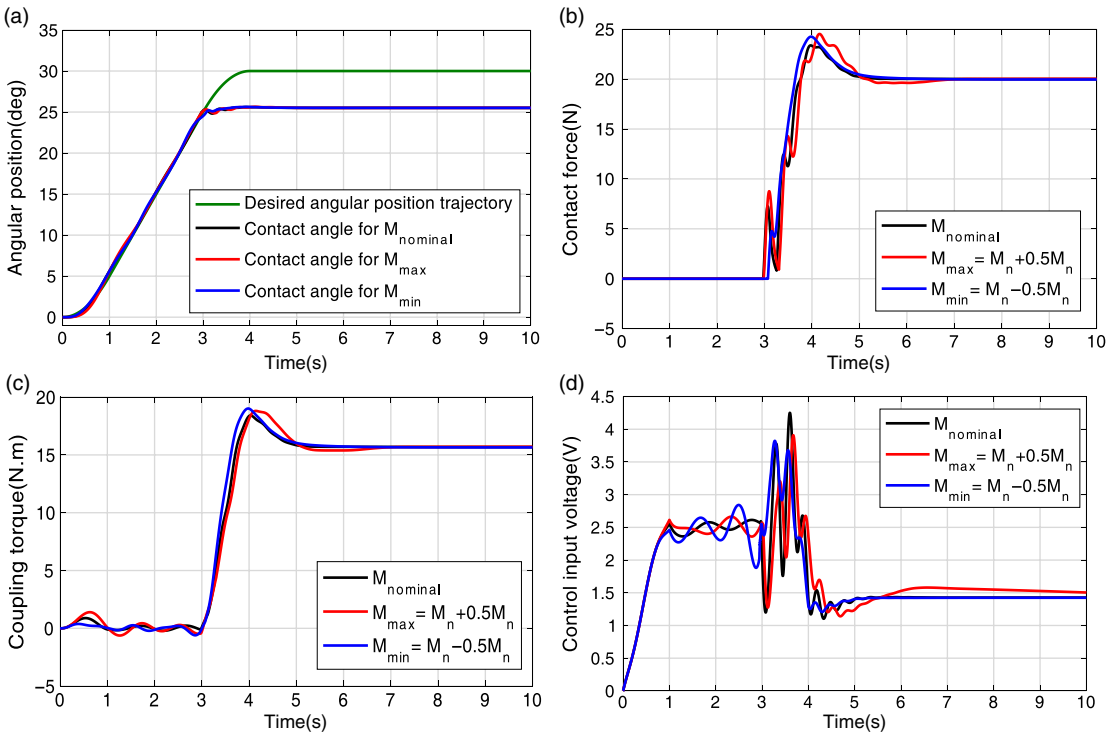

Fig. 11. System transient response in both free and constrained motion modes with 50 percent variation in the link mass value. (a) tracking of the prescribed desired trajectory (position control), (b) regulating the contact force to the desired value (force control), (c) coupling torque, and (d) control input voltage.

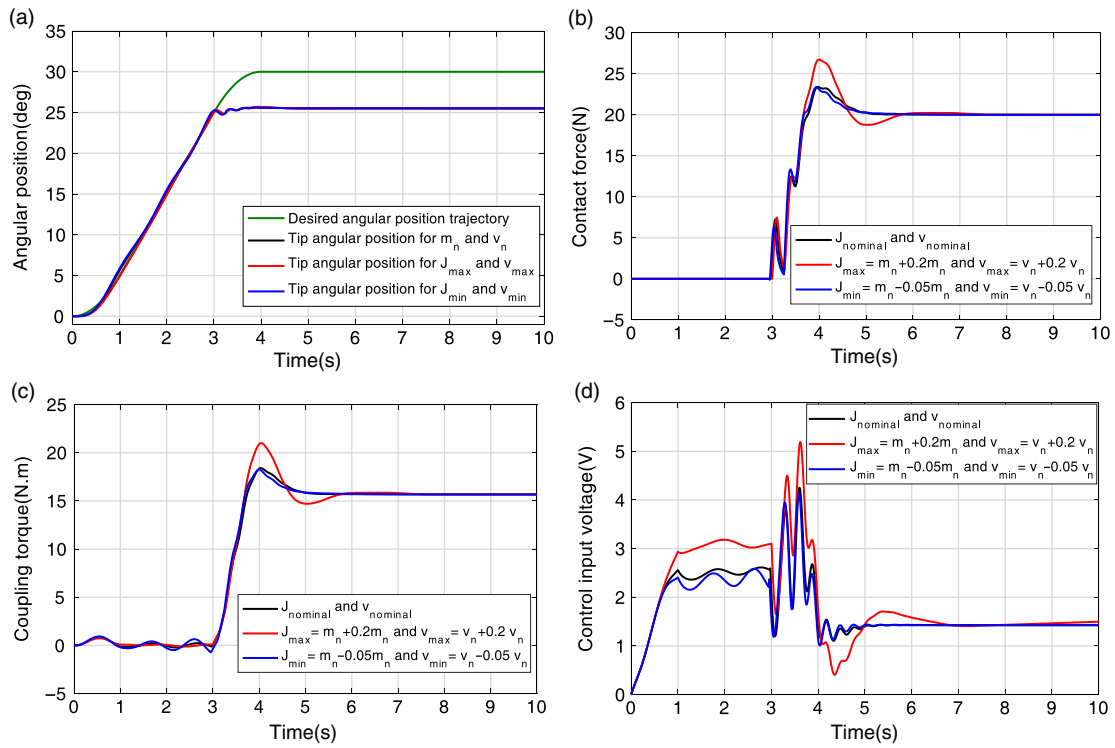

Fig. 12. System transient response in both free and constrained motion modes with 20 percent variation in the motor parameters.(a) tracking of the prescribed desired trajectory (position control), (b) regulating the contact force to the desired value (force control), (c) coupling torque, and (d) control input voltage.

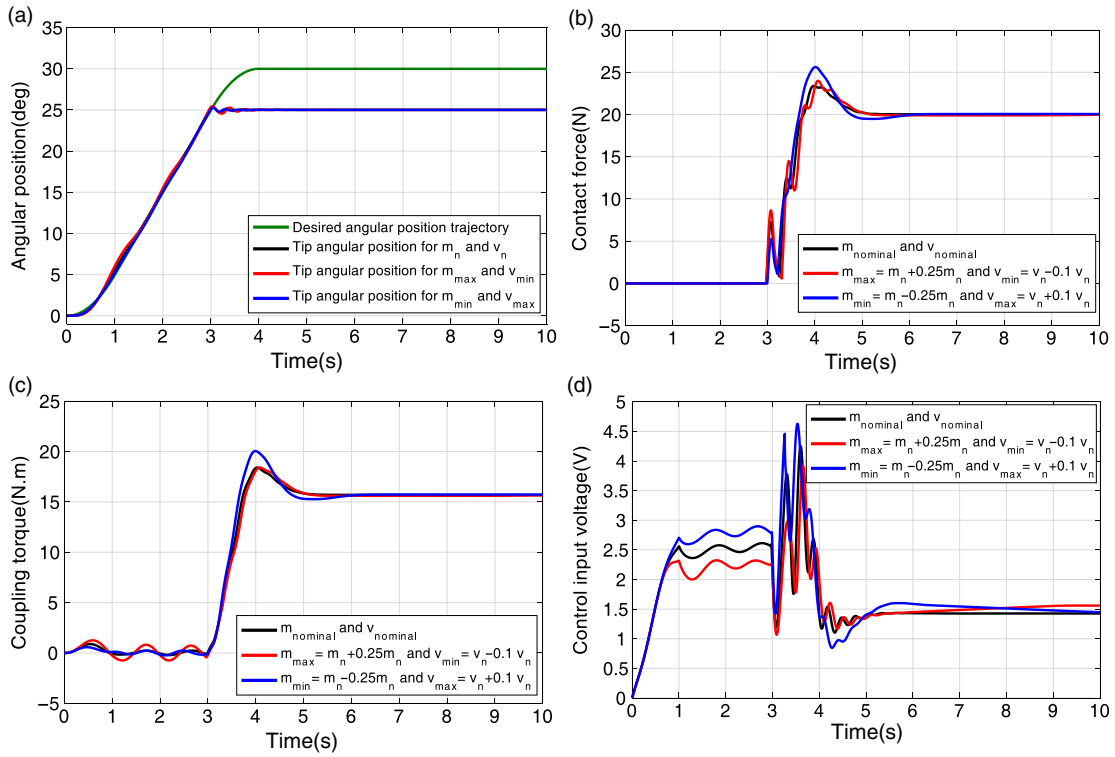

Fig. 13. System transient response in both free and constrained motion modes when payload mass and viscous friction vary simultaneously. (a) tracking of the prescribed desired trajectory (position control), (b) regulating the contact force to the desired value (force control), (c) coupling torque, and (d) control input voltage.

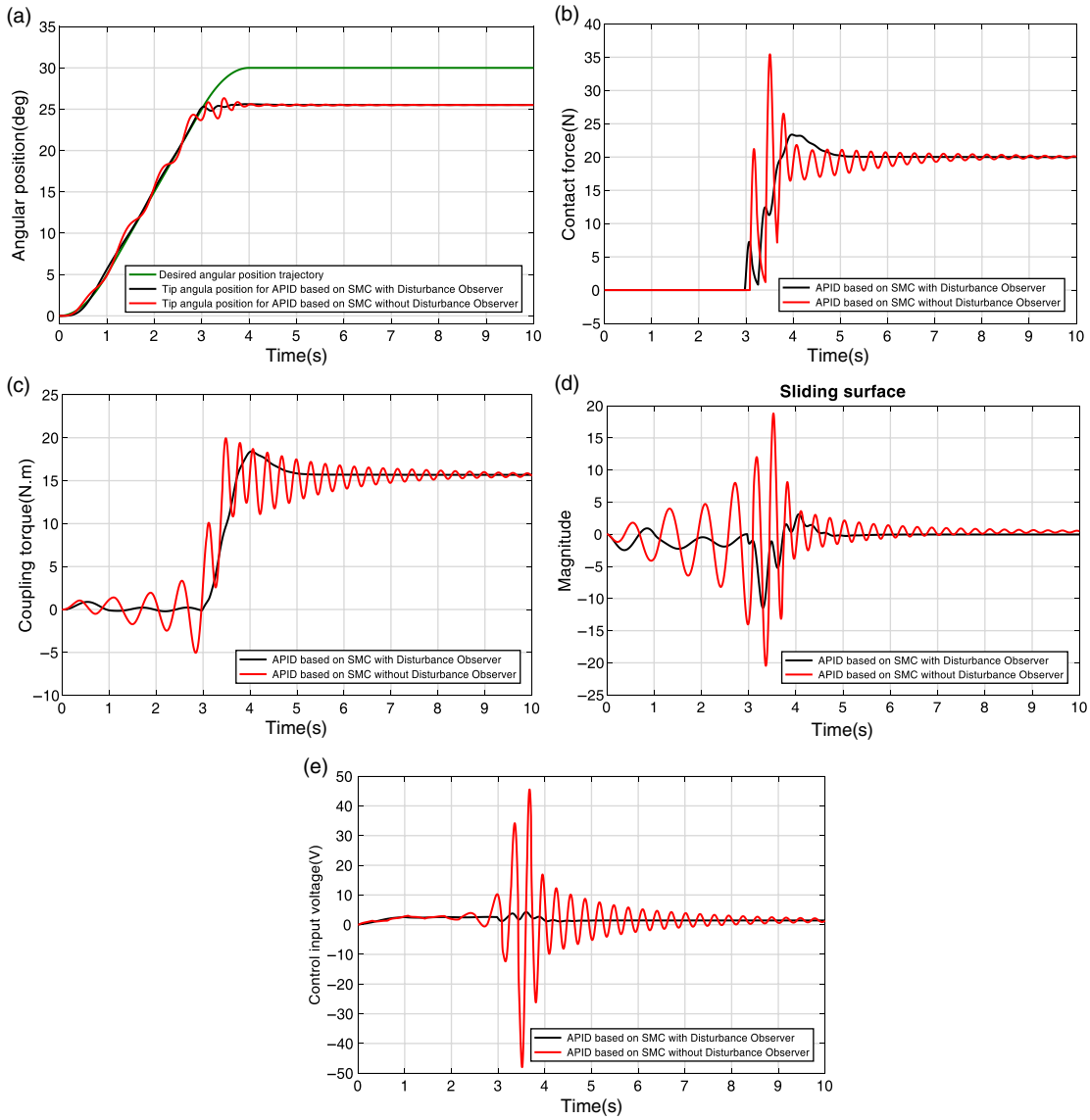

Fig. 14. System transient response in both free and constrained motion modes. (a) tracking of the prescribed desired trajectory (position control), (b) regulating the contact force to the desired value (force control), (c) coupling torque, and (d) control input voltage.

As can be seen from Figure 13(a), the free motion mode, the maximum deviation of the system response with respect to the nominal case (m_n, v_n) is almost 0.5° when m is equal to $m_{min} = m_n - 0.25m_n$ and v is equal to $v_{max} = v_n + 0.1v_n$. In the constrained motion mode, the steady-state error of the desired contact force regulating is zero.

Next, some simulation results are presented for the APIDSMC equipped by disturbances observer and the conventional APIDSMC.

6.6. Comparison between the proposed APIDSMC equipped by DO and the conventional APIDSMC

In this section, in order to investigate the capability of the APIDSMC equipped by disturbance observer (the proposed control approach) in comparison to the conventional APIDSMC without disturbance observer, several simulations are carried out for both constrained and unconstrained motions mode. Figure 14 illustrates the transient response of the system for both constrained and unconstrained motions phase. Figure 14(a) shows the desired trajectory tracking (position control in the free motion phase). Figure 14(b) depicts the transient response of the desired contact force regulating (force control in the constrained motion phase). Figure 14(c) shows the coupling torque applied

Table III. Results simulation of the proposed controller performances, in presence of the unknown Coulomb friction disturbances disturbances.

Position control strategy	e_p	e_f	**RMSE**	**RMSV**
APIDSMC equipped by DO	0.3132	0.2422	0.554	1.8618
APIDSMC without DO	0.6520	0.8060	1.4580	7.9284

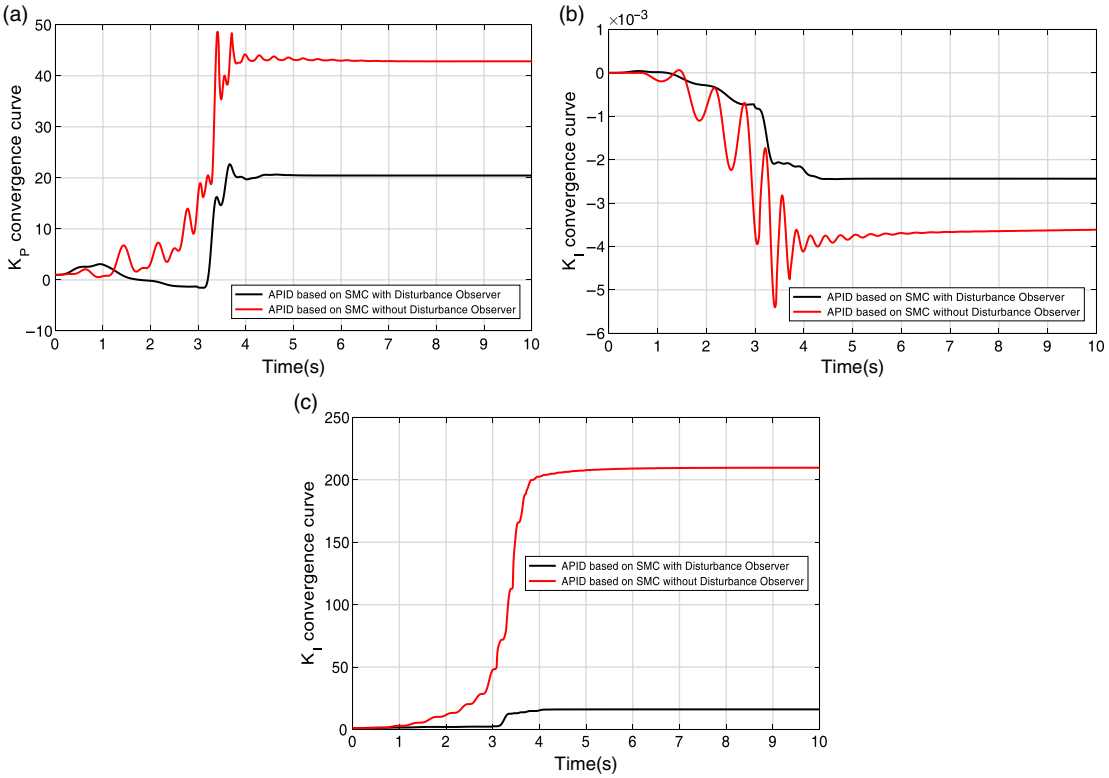

Fig. 15. Convegence of the PID controller. (a) K_P Convergence, (b) K_I Convergence. (c) K_D Convergence.

to the beam. Figure 14(d) illustrates the sliding surface. Figure 14(e) shows the control input voltage to the DC motor. The convergence of the control parameters of the PID controller is illustrated in Figure 15.

In order to compare the performance of the proposed APIDSMC controller equipped by disturbance observer over the conventional APIDSMC controller, the results of simulation are summarized in Table III. From Table III, it can be seen that the proposed APIDSMC controller equipped by disturbance observer has the smaller error and better tracking as compared with the conventional APIDSMC controller in both free and constrained motion mode.

As can be seen from Figure 14, the APIDSMC equipped with disturbance observer used in position control block (black curve) has better performance over the conventional APIDSMC without disturbance observer in both unconstrained and constrained movement mode. In the unconstrained motion phase, as depicted in Figure 14(a), the tip angular position (black curve) follows completely the desired angular position trajectory. Whereas, the simulation result of the conventional APIDSMC shows that the tip angular position (red curve) is unable to track the desired angular position trajectory. In the constrained motion phase, as illustrated in Figure 14(b), the desired contact force regulating is well done without any steady-state error. However, the conventional APIDSMC simulation result shows that the contact force oscillates around the desired value in the steady state. From Figure 14(c), it is obvious that the fluctuation amplitude of the coupling torque of the classical APIDSMC, specially in free motion phase, is much larger than that over the proposed control approach which is equipped by a disturbance observer. As shown in Figure 14(e), the control input voltage obtained in the proposed control method is much smoother and with less

oscillation amplitude than the control input obtained from the conventional APIDSMC. It should be noted that the disturbance observer used in the APIDSMC, apart from compensation of parameter uncertainties and unknown Coulomb friction disturbances, compensates the input disturbance caused by the flexibility of the link. Thus, the proposed APIDSMC equipped by disturbance observer has better performance as compared with the conventional APIDSMC in both free and constrained motion mode. Moreover, as shown in Figure 14(d), the chattering phenomenon has been eliminated using the proposed control approach along with the use of the smoothing function ($sat(\sigma)$) in the control law.

7. Conclusion

In this study, an adaptive robust impedance control was presented for a single-link flexible manipulator through APIDSMC scheme when it comes into contact with the environment at an unknown intermediate point. The proposed APIDSMC strategy was also equipped with a disturbance observer. In this work, it was assumed that the environment parameters (stiffness and damping coefficient) are known and the collision point between the environment and an intermediate point of the arm is unknown. Therefore, an algorithm was proposed to estimate the collision point. First, a dynamic model of a single flexible arm is derived based on a lumped masses model for the constrained maneuver mode. A comprehensive control strategy is, then, designed based on the model with collision at unknown intermediate point. The main contribution of this work is that the collision point is unknown. Moreover, only one model is used to design the controller that is applicable to both constrained and unconstrained motions. In our novel method, the contact length is estimated by a contact length estimation algorithm and then the controller switching will be done automatically from the unconstrained to the constrained movement mode. In this regard, the position-based impedance control scheme is provided for force tracking. The position controller is the main part of the proposed impedance control strategy in which an adaptive PID controller based on sliding mode control (APIDSMC) method is used. The combination of the adaptive control and the sliding mode control equipped by a disturbance observer is used to improve the performance of the system response. This hybrid system makes the system more robust against uncertainties. To investigate the performance and the capability of the proposed method, several simulations have been carried out under disturbance and variation in parameters of system consisting of variation in the environment parameters, the flexible link parameter, and the DC motor parameters. Real-time simulation was performed in MATLAB/Simulink to show the robustness and effectiveness of the proposed controller. The simulation results indicate the effectiveness of the proposed control scheme for both unconstrained and constrained movements mode where the flexible link interacting with the environment at unknown intermediate point. Besides, the proposed control system depicts robustness against the parameter variations of environment parameters, payload, and viscous friction variations in the defined range. Such that with 50% variation in the link weight, 20% variation in the DC motor parameters (viscous friction and inertia parameters), and for simultaneous variations in the weight of the link (25%) and in the viscous friction of the DC motor (10%), in the unconstrained motion mode, the maximum deviation from the nominal case is less than 0.7°, 0.8°, and 0.6°, respectively. In the constrained motion mode, the steady-state error of the desired contact force regulating is zero. Moreover, the variation of 10% in the dynamics parameters of the environment parameters (stiffness and damping coefficient) leads to a maximum of 1.14% error rate in the accuracy of force regulating. Besides, the practical implementation of the proposed control approach is quite possible due to the control input voltage features which is smooth and never exceeds the positive or negative saturation voltages (the saturation periods which supplies the motor at 10 and −10 V).

Declaration of Conflicting Interest

The authors declared no potential conflicts of interest with respect to the research, authorship, and/or publication of this article.

Funding

The author(s) received no financial support for the research, authorship, and/or publication of this article.

References

1. F. Wangć and Y. Gao, *Advanced Studies of Flexible Robotic Manipulators, Modeling, Design, Control and Applications* (World Scientific, New Jersey, 2003). ISBN: 978-981-279-672-1.
2. O. Sawodny, H. Aschemann and A. Bulach, "Mechatronical Designed Control of Fire Rescue Turnable Ladders as Flexible Link Robots," *Proceedings of the IFAC 15th Triennial World Congress*, Barcelona, Spain (2002).
3. D. Feliu-Talegon and V. Feliu-Batlle, "Improving the position control of a two degrees of freedom robotic sensing antenna using fractional-order controllers," *Int. J. Control* **90**(6), 1256–1281 (2017).
4. V. Feliu-Batlle, D. Feliu-Talegon and C. F. Castillo-Berrio, "Improved object detection using a robotic sensing antenna with vibration damping control," *Sensors* **17**(4), 1–28 (2017).
5. S. K. Dwivedyć and P. Eberhard, "Dynamic analysis of flexible manipulators, a literature review," *Mech. Mach. Theory* **41**(7), 749–777 (2006).
6. K. Lochan, B. K. Royand and B. Subudhi, "A review on two-link flexible manipulators," *Ann. Rev. Control* **42**, 346–367 (2016).
7. S. Mobergć, Modeling and Control of Flexible Manipulators, *PhD thesis,* Linköping University, SE-581 83 Linköping, Sweden (2010).
8. C. T. Kiang, A. Spowage and C. K. Yoong, "Review of control and sensor system of flexible manipulator," *J. Intell. Robot. Syst.* **77**(1), 187–213 (2015).
9. A. Benosman and G. L. Vey, "Control of flexible manipulators: a survey," *Robotica* **22**(5), 533–545 (2004).
10. N. Hogan, "Impedance control: An approach to manipulation: Part1, Part2, Part3," *J. Dyn. Syst. Meas. Cont.* **107**, 1–24 (1985).
11. V. Feliu, F. J. Castillo, F. Ramos and J. A. Somolinos, "Robust tip trajectory tracking of a very lightweight single-link flexible arm in presence of large payload changes," *Mechatronics* **22**(5), 594–613 (2012).
12. C. F. Castillo-Berrio, S. N. Engin and V. Feliu-Batlle, "A study on the tip tracking control of a single flexible beam," *Trans. Inst. Meas. Cont.* **38**(5), 602–617 (2017).
13. G. Mamani, J. Besedas and V. Feliu, "Sliding mode tracking control of a very lightweight single-link flexible robot robust to payload changes and motor friction," *J. Vibr. Cont.* **18**(8), 1141–1155 (2012).
14. D. Heck, A. Saccon, N. V. D. Wouw and H. Nijmeijer, "Guaranteeing stable tracking of hybrid position-force trajectories for a robot manipulator interacting with a stiff environment," *Automatica* **63**, 235–247 (2016).
15. I. Payo, V. Feliu and O. D. Cortazar, "Force control of a very lightweight single-link flexible arm based on coupling torque feedback," *Mechatronics* **19**(3), 334–347 (2009).
16. J. C. Cambera and V. Feliu-Batlle, "Input-state feedback linearization control of a single-link flexible robot arm moving under gravity and joint friction," *Robotics and Autonomous Systems* **88**, 24–36 (2017).
17. T. Endo, M. Sasaki and F. Matsuno, "Contact-force control of a flexible Timoshenko arm," *IEEE Trans. Autom. Cont.* **62**(2), 1004–1009 (2017).
18. C. Murrugarra, O. D. Castrob, J. C. Griecoc and G. Fernandezc, "A general scheme implicit force control for a flexible-link manipulator," *Submitted to Journal of Nonlinear Analysis: Hybrid Systems* (2017).
19. J. Becedas, I. Payo and V. Feliu, "Two-flexible-fingers gripper force feedback control system for its application as end effector on a 6-DOF manipulator," *IEEE Trans. Robot.* **27**(3), 599–615 (2011).
20. M. M. Fateh and R. Babaghasabha, "Impedance control of robots using voltage control strategy," *Nonlinear Dyn.* **74**(1), 277–286 (2013).
21. S. Jung, T. C. Hsia and R. G. Bonitz, "Force tracking impedance control of robot manipulators under unknown environment," *IEEE Trans. Cont. Syst. Technol.* **12**(3), 474–483 (2004).
22. T. Lasky and T. C. Hsia, "On Force-Tracking Impedance Control of Robot Manipulators," *Proceedings of the IEEE International Conference on Robotics and Automation*, Sacramento, CA, USA (1991) pp. 274–280.
23. H. Seraji and R. Colbaugh, "Force Tracking in Impedance Control," *Proceedings of the IEEE International Conference on Robotics and Automation*, Atlanta, GA, USA (1993) pp. 499–506.
24. K. Lee and M. Buss, "Force Tracking Impedance Control with Variable Target Stiffness," *Proceedings of the 17th World Congress The International Federation of Automatic Control*, Seoul, Korea (2008) pp. 6751–6756.
25. Y. Li, S. S. Ge, C. Yang, "Learning impedance control for physical robot-environment interaction," *Int. J. Cont.* **85**(2), 182–193 (2012).
26. Y. Li, S. S. Ge, "Impedance learning for robots interacting with unknown environments," *IEEE Trans. Cont. Syst. Technol.* **22**(4), 1422–1432 (2014).
27. C. Semini, V. Barasoul, T. Boaventura, M. Frigerio, M. Focchi, D. G. Caldwell and J. Buchli, "Towards versatile legged robots through active impedance control," *Int. J. Robot. Res.* **34**(7), 1003–1020 (2015).
28. W. He, Y. Dong and C. Sun, "Adaptive neural impedance Control of a robotic manipulator with input saturation," *IEEE Trans. Syst. Man Cybern. Syst.* **46**(3), 334–344 (2016).
29. H. Mehdi and O. Boubaker, "Robust impedance control-based Lyapunov-Hamiltonian approach for constrained robots," *Int. J. Adv. Robot. Syst.* **12**(12), 1–12 (2015).
30. G. R. Vossoughi and A. Karimzadeh, "Impedance control of a flexible link robot for constrained and unconstrained maneuvers using Sliding Mode Control (SMC) method," *Scientia Iranica* **14**(1), 33–45 (2007).
31. G. R. Vossoughi and A. Karimzadeh, "Impedance control of a two degree-of-freedom planar flexible link manipulator using singular perturbation theory," *Robotica* **24**(2), 221–228 (2006).

32. T. Wongratanaphisan and M. O. T. Cole, "Robust impedance control of a flexible structure mounted manipulator performing contact tasks," *IEEE Trans. Robot.* **25**(2), 445–451 (2009).
33. Q. Xu, "Robust impedance control of a compliant microgripper for high-speed position/force regulation," *IEEE Trans. Ind. Electron.* **62**(2), 1201–1209 (2015).
34. A. Fayazi, N. Priz, A. Krimpour and S. H. Hosseinnia, "Robust position-based impedance control of lightweight single-link flexible robots interacting with the unknown environment via fractional order sliding mode controller," *Robotica* **36**(12), 1920–1942 (2018).
35. E. Bayo, "A finite-element approach to control the end-point motion of a single-link flexible robot," *J. Robot. Syst.* **4**(1), 63–75 (1987).
36. V. Feliu, K. Rattan and N. Brown, "Modeling and control of single-link flexible arms with lumped masses," *J. Dyn. Syst. Meas. Cont.* **114**(1), 59–69 (1992).
37. R. H. Cannon and E. Schmitz, "Initial experiments on the end-point control of a flexible robot," *Int. J. Robot. Res.* **3**(3), 62–75 (1984).
38. H. Yang, J. Liu and X. Lan, "Observer design for a flexible-link manipulator with PDE model," *J. Sound Vibr.* **341**, 237–245 (2015).
39. T. Jiang, J. Liu and W. He, "A robust observer design for a flexible manipulator based on a PDE model," *J. Vibr. Cont.* **23**(6), 871–882 (2017).
40. W. H. Chen, "Nonlinear disturbance observer-enhanced dynamic inversion control of missiles," *J. Guid. Cont. Dyn.* **26**(1), 161–166 (2003).
41. M. Corless and G. Leitman, "Continuous state feedback guaranteeing uniform ultimate boundedness for uncertain dynamic systems," *IEEE Trans. Autom. Cont.* **26**(5), 1139–1144 (1981).
42. V. S. Deshpande, B. Mohan, P. D. Shendge and S. B. Phadke, "Disturbance observer based sliding mode control of active suspension systems," *J. Sound Vibr.* **333**(11), 2281–2296 (2014).
43. I. Payo, F. Ramos, O. D. Cortazar and V. Feliu, "Experimental validation of nonlinear dynamic models for single-link very flexible arms," *Proceedings of the IEEE Conference on Decision and Control, and the European Control Conference*, Seville, Spain (2005) pp. 5304–5309.

Appendix A. Convergence Proof of the Contact Length Estimation Algorithm

Let us again consider the contact length estimation algorithm (Equation(24)) as follows:

$$\lambda_{new} = \lambda_{old} + \alpha \left(\Gamma_l^f - \Gamma_l \right) \tag{A.1}$$

We define the error between the coupling torque of the fictitious arm (Γ_l^f) and the measured coupling torque of the real arm (Γ_l) as follows:

$$e_\Gamma = \Gamma_l^f - \Gamma_l \tag{A.2}$$

Now we make claim that if the e_Γ goes down to zero ($\Gamma_f^l \to \Gamma_l$), then the λ_{old} convergences to λ_{new}. To prove this claim, we pursue the following equations. By substituting (5) in (A.2) the the Eq. (A.2) can be rewritten as:

$$e_\Gamma = ml^2\ddot{\theta}_t + k_e\lambda_{new}^2 l^2 \left(\theta_c - \theta_e\right) + v_e\lambda_{new}^2 l^2\dot{\theta}_c - ml^2\ddot{\theta}_t - k_e\lambda_{old}^2 l^2 \left(\theta_c - \theta_e\right) - v_e\lambda_{old}^2 l^2\dot{\theta}_c = 0 \tag{A.3}$$

After simplifying, the Eq. (A.3) can be rewritten as:

$$l^2\left(\lambda_{new}^2 - \lambda_{old}^2\right)\left(k_e\theta_c + v_e\dot{\theta}_c\right) = 0 \Rightarrow k_e\theta_c + v_e\dot{\theta}_c = 0 \Rightarrow \theta_c = k_e\, e^{-v_e t}, \quad t > 0 \tag{A.4}$$

This implies that θ_c will tend to zero ($\theta_c \to 0$) as time goes to infinity ($t \to \infty$). Therefore, we can claim that the ($e_\Gamma \to 0$) and then λ_{old} convergences to λ_{new}.